

Validation of line-of-sight water vapor measurements with GPS

John Braun, Christian Rocken, and Randolph Ware

GPS Research Group, University Corporation for Atmospheric Research, Boulder, CO

Abstract. We present a direct comparison of nonisotropic, integrated water vapor measurements between a ground-based Global Positioning System (GPS) receiver and a water vapor radiometer (WVR). These line-of-sight water vapor observations are made in the straight line path between a ground station and a GPS satellite. GPS double-difference observations are processed, and the residual line-of-sight water vapor delays are extracted from the double-difference residuals. These water vapor delays contain the nonisotropic component of the integrated water vapor signal. The isotropic component is represented by the zenith precipitable water vapor measurement and can be scaled to a specific elevation angle based on a mapping function. The GPS observations are corrected for station-dependent errors using site-specific multipath maps. The resulting measurements are validated using a WVR which pointed in the direction of the observed satellites. The double-difference technique used to make these water vapor observations does not depend on accurate satellite clock estimates. Therefore it is especially well suited for near-real-time application in weather prediction and allows for sensing atmospheric structure that is below the noise level of current satellite and receiver clock errors. This paper describes the analysis technique and provides precision estimates for the GPS-measured nonisotropic water vapor as a function of elevation angle for use with data assimilation systems.

1. Introduction

This study is motivated by the need for accurate measurements of atmospheric water vapor with precise spatial and temporal resolution. Applications of these observations include weather prediction [Emanuel *et al.*, 1996; Dabberdt and Schlatter, 1996] and climate research [Stokes and Schwartz, 1994]. Experiments have shown that zenith integrated precipitable water (PW) can be readily obtained with better than 2 mm absolute accuracy using GPS instruments [e.g., Bevis *et al.*, 1992; Rocken *et al.*, 1993, 1995, 1997]. The assimilation of PW data into numerical weather models has been shown to significantly improve the initial state and model prediction of rainfall [Guo *et al.*, 2000]. However, PW measurements do not provide any information on the spatial distribution of water vapor. The integrated amount of precipitable water along each path from an individual satellite to a receiver is called slant water (SW) [Ware *et al.*, 1997]. GPS PW measurements are essentially averages over all SW measurements which are mapped to the equivalent zenith value and averaged over a period of time typically ranging from between 5 and 30 min. Because of this averaging, the nonisotropic component of SW is removed when computing PW. For a single site, recording measurements every 30 s from 5-12 satellites, there are between 300 and 750 observations averaged in a 30 min estimate of PW. While PW measurements contain no information about the distribution of the water vapor at a site, SW measurements do. SW measurements, how-

ever, are more difficult to measure than PW because they do not benefit from averaging and are thus strongly affected by noise due to instabilities of the GPS receiver and transmitter oscillators, satellite orbit error, site multipath, and antenna effects.

SW observations have the potential to be useful in reconstructing the three-dimensional water vapor field if they can be successfully assimilated into numerical weather models [MacDonald and Xie, 2000]. Assimilation techniques for this data type are currently under development at the National Center for Atmospheric Research (NCAR). For data assimilation the error estimate of the measurement is as important as the measurement itself [Kuo *et al.*, 1996; Guo *et al.*, 2000]. In preparation for future use of SW in weather prediction we describe how the nonisotropic component of SW can be obtained from the residuals of modeled GPS observations and what the error of these water vapor measurements is as a function of satellite elevation angle. Other applications of SW measurements are in the calibration of interferometric synthetic aperture radar (InSAR) images [Hanssen *et al.*, 1999] and tomographic modeling techniques [Howe *et al.*, 1998; Ruffini *et al.*, 1999; Elosgui *et al.*, 2000]. This paper first describes how we retrieve the nonisotropic component of SW from our GPS analysis. Then we describe a technique to reduce the effect of site multipath on these observations. Finally, they are compared with independent observations from a water vapor radiometer (WVR) that was located near the GPS antenna and pointed at the observed GPS satellites.

2. Estimation of SW From GPS

Slant water vapor delay (SWD_i^m) is defined as the path integral of atmospheric refractivity due to water vapor $N(w)$, between the receiving antenna i and the transmitting GPS satellite m .

$$\text{SWD}_i^m = 10^{-6} \int_{\text{ANT}_i}^{\text{GPS}^m} N(w) ds. \quad (1)$$

The refractivity of atmospheric water vapor is a function of the partial pressure of water vapor e_w (millibars) and the temperature T (Kelvin) [Bevis *et al.*, 1994]:

$$N(w) \approx k \frac{e_w}{T^2}, \quad (2)$$

where the constant $k = 3.73 \times 10^5 \text{ K}^2/\text{mbar}$.

Integrated slant water vapor ISW_i^m is defined as the integrated water vapor density ρ_w along the ray path between the receiving antenna i and the transmitting GPS satellite m and, as shown below, is linearly related to the slant water vapor delay [see, e.g., Hogg *et al.*, 1981; Bevis *et al.*, 1992].

$$\text{ISW}_i^m = \int_{\text{ANT}_i}^{\text{GPS}^m} \rho_w ds. \quad (3)$$

Using the ideal gas law with the gas constant for water vapor, $R_v = 461.5 \text{ J}/(\text{kgK})$, we can rewrite the integrated slant water vapor as a function of vapor pressure (e_w) and temperature (T) along the line integral from the receiving GPS antenna i to the transmitting satellite m .

$$\text{ISW}_i^m = \frac{1}{R_v} \int_{\text{ANT}_i}^{\text{GPS}^m} \frac{e_w}{T} ds. \quad (4)$$

Atmospheric scientists oftentimes relate the amount of integrated water vapor in the atmosphere (in the zenith direction) to the length of an equivalent column of liquid water. This is done by dividing the zenith integrated water vapor by the density of liquid water ρ , and is referred to as precipitable water (PW). In a similar manner, we define the slant water SW_i^m as the length of an equivalent column of liquid water for the ray path between a GPS receiver i and satellite m . SW_i^m is then the integrated slant water vapor divided by the density of liquid water ($\text{SW}_i^m = \text{ISW}_i^m / \rho$).

The ratio of slant water to the slant water vapor delay is known as Π . It can be expressed as

$$\Pi = \frac{\text{SW}_i^m}{\text{SWD}_i^m} = \frac{\frac{1}{\rho R_v} \int_{\text{ANT}_i}^{\text{GPS}^m} \frac{e_w}{T} ds}{10^{-6} k \int_{\text{ANT}_i}^{\text{GPS}^m} \frac{e_w}{T^2} ds} = \frac{10^6}{\rho k R_v} T_m, \quad (5)$$

where T_m is called the mean temperature of the atmosphere [Davis *et al.*, 1985] and can be computed from the temperature profile above a GPS receiver. It has been shown that T_m is highly correlated with the surface temperature and can be approximated by $T_m = 70.2 + 0.72T_s$ [Bevis *et al.*, 1994]. This approximation was obtained through an analysis of radiosonde data collected from stations within the United States and should be accurate to $\sim 2\%$ for all weather conditions. We used this approximation in the study presented here. The typical value of Π is 0.15, implying that 1 mm of slant water corresponds to a slant water vapor delay of ~ 6.5 mm. In this paper we will henceforth refer to slant water as the equivalent amount of liquid water in units of millimeters. It should be mentioned that to eliminate any errors that might be introduced from assumptions about T_m , the slant water vapor delay can be used in place of slant water for assimilation into numerical weather models. This paper discusses slant water because it can be directly validated against measurements from a WVR.

GPS observations are affected by the delay due to both the wet and dry components of the atmosphere. The dry delay is commonly removed through the use of surface observations of pressure and temperature [Elgered *et al.*, 1991] and will not be extensively discussed in this paper.

The slant water vapor delay SWD_i^m can be divided into two components:

$$\text{SWD}_i^m = \frac{1}{\Pi} \left[\frac{\text{PW}}{m(\theta_i^m)} + S_i^m \right], \quad (6)$$

where $m(\theta_i^m)$ is the mapping function that scales the delay at an elevation angle θ_i^m from station i to satellite m [Niell, 1996] to zenith. The first term on the right-hand side of (6), the isotropic component of slant water, can be computed from the PW measurements. The second term, S_i^m , represents the nonisotropic component of the slant water and is the focus of this paper. The term is zero when the atmosphere is perfectly isotropic, negative when the GPS signal passes through a region of low water vapor content relative to the PW estimate, and positive when it passes through a region of high water vapor content relative to the estimate based on PW. Typically,

the magnitude of the second term is less than 20% of the PW term [see, e.g., *Rocken et al.*, 1991; *Jarlemark et al.*, 1998]. For this reason we present observations of S_i^m only, neglecting the PW component. We measure S_i^m by accurately modeling and correcting for the clock delays, geometric delays, hydrostatic delay, ionospheric delay, and the isotropic part of the wet delay. After these components of the GPS measurements are correctly removed by the modeled observations, the residual (observation minus model) is the delay caused by the nonisotropic component of the SW, or S_i^m .

Modeling of the GPS observations can be done with either precise point positioning (PP) [*Zumberge et al.*, 1997] or with double-difference (DD) processing [*Beutler et al.*, 1996]. The PP technique has the advantage that the line-of-sight observations from the receiving antenna to each transmitting satellite are individually modeled. The resulting residuals are then the nonisotropic component of the wet delay. The disadvantage of PP analysis is that accurate receiver and satellite clock estimates are needed. Typically, satellite clock values are computed from a large, often global, GPS tracking network in the same processing step that the orbits are computed. These satellite clock values are then distributed in the same file as the orbits. The receiver clock is included in the estimation process as a random walk parameter when PW is estimated. In addition to the receiver clock estimate, it is not possible to resolve the integer carrier phase ambiguities in PP. The DD technique removes GPS transmitter and receiver clock errors and allows for ambiguity resolution by differencing simultaneous observations from two sites and two satellites. The disadvantage is that the resulting residual is a combination of four observations instead of one. Because DD processing eliminates clock estimation and allows for ambiguity resolution, it is more sensitive to small variations in S_i^m than the PP technique. This is especially important for weather prediction applications because the nonisotropic component of SW can be small and results must be available in close to real time when accurate clock estimates are generally not available.

The technique to transform double-difference residuals into line-of-sight residual delays (which can then be converted into nonisotropic slant water observations) for an individual ray path between a transmitting satellite and a receiving antenna is explained in detail by *Alber et al.* [2000]. In brief, the technique depends on two assumptions. First, the sum of the single-difference residuals to all satellites visible at each observation epoch for a pair of stations in a baseline must be equal to zero. This

implies that the observations must be sufficiently well modeled so that for every baseline in the solution, the sum of the unmodeled components of the single-difference observations is equal to zero. Errors in this assumption arise when station biases are left in the solution. This can occur when the mean atmospheric delay (caused by PW) is not removed or when incorrectly resolving carrier phase ambiguities. The second assumption requires that the sum of the unmodeled portions of the observations from all the stations in the network to a single satellite is zero. Errors in the assumptions, and their effects on the individual line-of-sight residuals, are reduced by increasing the number of stations processed in the network and by increasing baseline length to avoid common mode errors. The resulting line-of-sight residuals contain unmodeled atmospheric delay, antenna phase center variations, and station multipath. In order to retrieve high-quality atmospheric signals from the line-of-sight residuals, the antenna phase center variations need to be accurately modeled, and the multipath errors must be kept to a minimum. After the residuals have been corrected for these station-specific errors, they can be multiplied by Π to become the S_i^m observations.

3. Experiment Description and Analysis

Data were analyzed from eight locations spanning 3 days, May 21-23, 1996. Six of the stations are part of the National Oceanic and Atmospheric Administration's (NOAA) Forecast Systems Laboratory (FSL) wind profiler network [*Gutman et al.*, 1995]. These six stations are equipped with Trimble 4000 SSE receivers and Trimble 4000ST L1/L2 antennas. The distances between the NOAA FSL stations are a few hundreds of kilometers, with locations in Colorado, New Mexico, Kansas, and Oklahoma. Two additional GPS stations were used, both equipped with Trimble 4000 SSI receivers and 85 cm choke ring antennas [*Alber et al.*, 1997]. One of these was essentially collocated with the NOAA FSL station in Platteville, Colorado. For these two Platteville stations the distance between the two antennas was 100 m. The PW and S_i^m results from these two stations were compared for consistency. The second additional GPS station was operated at the Table Mountain Gravity Observatory just north of Boulder, Colorado. Table Mountain is approximately 43 km west of Platteville. Radiometrics WVR-1100 radiometers with elevation and azimuth pointing capability were operated at Platteville and Table Mountain. In an earlier experiment, data from two collocated WVR-1100 radiometers were compared and produced equivalent PW measurements with an RMS

difference of 2.8 mm and a bias of 1.8 mm [Ware *et al.*, 1993]. The GPS and radiometer data from these two sites have been analyzed for previous studies [Alber *et al.*, 1997; Ware *et al.*, 1997], including the sensing of double-differenced slant water observations. The average PW at Platteville and Table Mountain during the observation period was 18 mm, with variations ranging from 15 to 30 mm.

3.1. GPS Data Analysis

All GPS data were processed using the Bernese GPS software version 4.0 [Beutler *et al.*, 1996]. Final orbits from the International GPS Service [Kouba, 1998] were used. To remain consistent with the orbits, station coordinates were estimated using the International Terrestrial Reference Frame 1993 (ITRF93). In both the positioning and the atmospheric analysis, data were collected and processed at 30 s intervals and all available data above 10° elevation were used. For the atmospheric analysis the station coordinates were constrained to 0.1 mm. This

tight constraint essentially fixed their position to their previously estimated values. The vertical coordinate repeatability for the 3 days of solutions was 2-3 mm for the two stations. Vertical position errors and PW errors are correlated. For example, a 3 mm vertical error introduces a 0.07 mm error in PW when analyzing data with a 10° elevation mask [Beutler *et al.*, 1988]. While coordinate errors cause errors in PW, they will not affect the nonisotropic component of SW as defined in (6). Surface pressure measurements were used with a modified Saastamoinen model to remove the dry delay. PW estimates for each station were computed using all observations collected during a half hour interval and the wet Niell mapping function [Niell, 1996]. The double-difference residuals were inverted into line-of-sight residuals through a separate program and the technique of Alber *et al.* [2000]. They were then converted into nonisotropic SW observations (S_i^m) using a Π value computed from observed surface temperature (section 2).

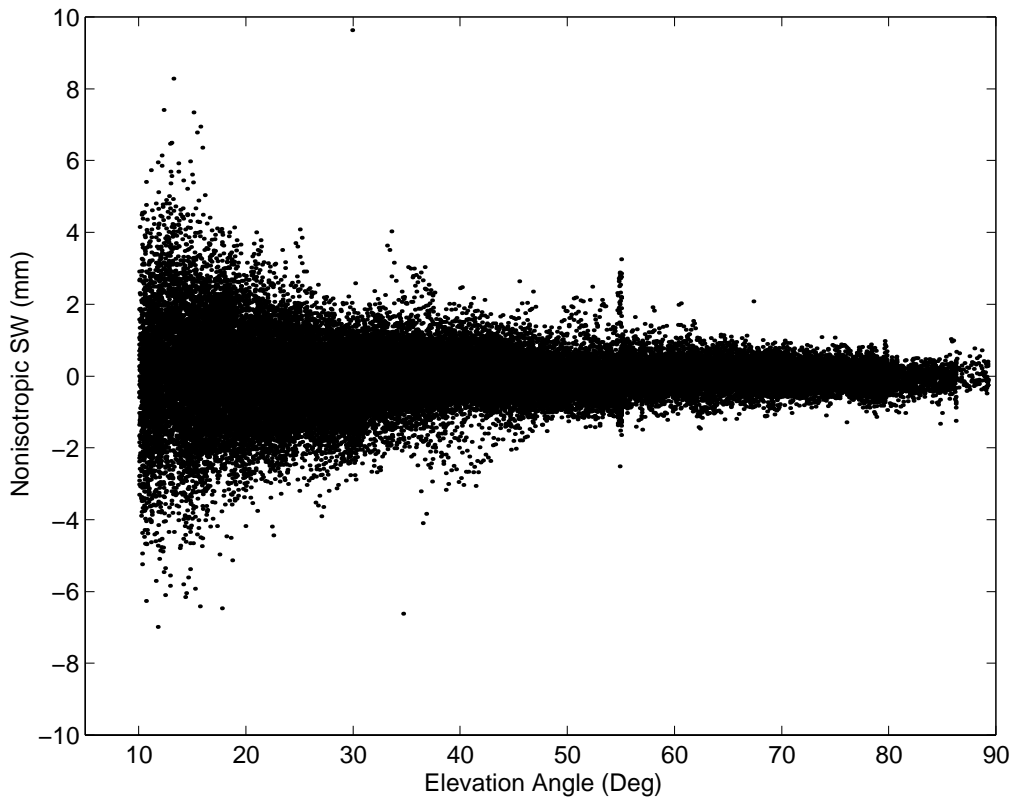


Figure 1. Nonisotropic SW for the Table Mountain GPS station plotted as a function of elevation angle. The observations are from the solution using the choke ring antenna and multipath map. All observations are plotted for all 3 days of data analyzed.

3.2. Stacking of Residuals for Multipath Suppression

The retrieved S_i^m observations can contain, in addition to the atmospheric signal, noise from ground reflections near the GPS antenna and from direction-dependent variations in the GPS antenna's phase response. These noise sources, to first order, are a function of the elevation and azimuth angle of the incoming GPS signal and repeat on a daily basis according to the direction of the incident ray path. To minimize these errors, the line-of-sight residuals were averaged for the 3 days to produce a multipath map. This map was then incorporated into the modeled observations during processing. The use of this map was modestly successful, and the results of its use will be discussed in sections 5 and 7.

3.3. Processing of Water Vapor Radiometer Observations

The radiometers were operated so that they would measure SW in the direction of all GPS satellites which

were greater than 10° above the horizon. During a typical configuration there would be between 5 and 12 satellites in view. The radiometers would cycle through each of the satellites, pointing in the direction of a particular one approximately every 8 min. The SW observations were transformed into PW measurements using the function $PW(\theta_i^m) = m(\theta_i^m)SW(\theta_i^m)$, with the mapping function $m(\theta_i^m) = \sin(\theta_i^m)$. This simple mapping function should not degrade the accuracy of the WVR observations because the WVR measures water vapor from atmospheric brightness temperature with a 5° beam width.

During the 3 days there were at least two rain events. The radiometer SW measurements during these times were corrupted by liquid water collecting on the instrument window or by scattering effects from hydrometeors [Zhang *et al.*, 1999]. It was therefore necessary to discard these sections of data. The radiometer data were binned into half-hour time windows to estimate PW and remove the isotropic component of SW. This time window was

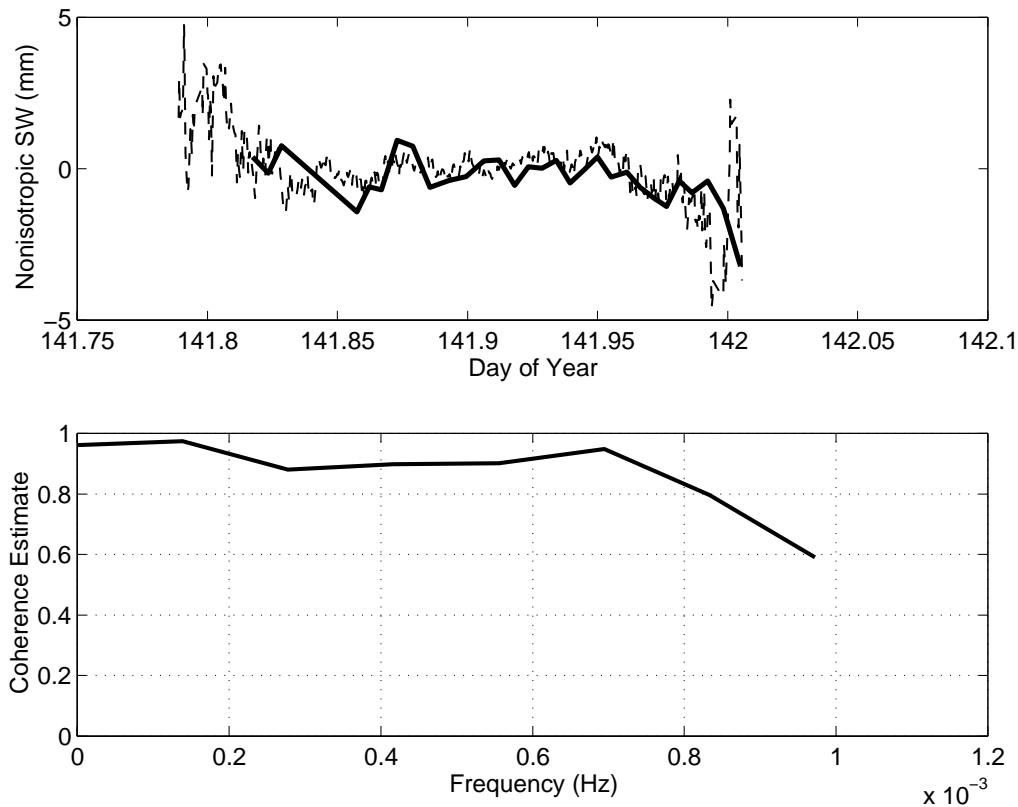


Figure 2. Nonisotropic SW for a single satellite track for the Table Mountain GPS station. In the top panel, GPS observations (in 30 s intervals) are plotted as the dashed line, and WVR observations are plotted as the thicker solid line (8 min intervals). The coherence between the GPS (decimated to 8 min intervals) and WVR time series is plotted in the bottom panel as a function of frequency in hertz. The GPS observations are from the solution using the choke ring antenna, multipath map, and 2 min filter.

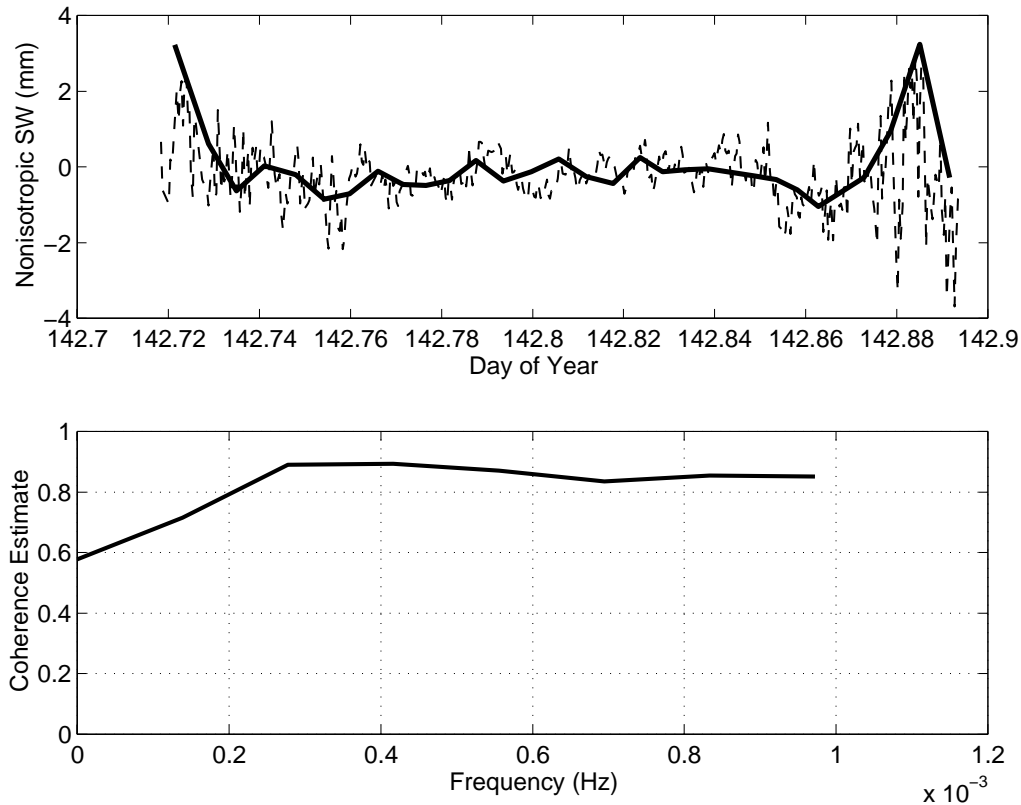


Figure 3. Nonisotropic SW for a single satellite track for the Platteville GPS station. The description of the panels is the same as in Figure 2.

chosen to match the one used for the GPS PW estimates. For each half hour the mean PW value was calculated and subtracted from the individual radiometer measurements, leaving only the S_i^m component. To eliminate data corrupted by liquid water, all the S_i^m measurements for each 30 min time window were scaled to zenith, and the root-mean-square (RMS) of each window was computed. The RMS of the entire 3 days of S_i^m observations was also computed. Any 30 min set of S_i^m observations whose RMS value was larger than the RMS for the entire 3 day data set was removed from the comparison. While limiting the total water vapor variability, it guaranteed the removal of any portions of data which might have been corrupted by liquid water.

4. Results

During the 3 days of observations there were 183 satellite tracks where both the GPS and WVR instruments collected a sufficient amount of data to compare observa-

tions. The GPS-derived S_i^m measurements are plotted in Figure 1 for the GPS station at Table Mountain.

Figure 1 represents the second, or nonisotropic, term in (6). The PW portion of the signal is not included to better illustrate the variations in S_i^m . Figure 1 shows a peak variability of up to 5 mm, while the mean PW estimate for these data was 18 mm. When this nonisotropic term is scaled to the equivalent zenith value, the largest S_i^m observations corresponded to less than 5% of the mean PW value. The lack of large-magnitude S_i^m observations can be attributed to the dry, homogeneous atmospheric conditions which often exist over the Colorado Front Range area at an altitude of ~1500 m. Radiometric studies by *Rocken et al.* [1991] and *Davis et al.* [1993] have reported nonisotropic components of SW as large as 20% of the equivalent PW values. Davis et al. report variations of S_i^m to be as large as 4.5 mm of the equivalent PW (or 17.3 mm of S_i^m at 15° elevation) along the Swed-

Table 1. RMS of S_i^m Observation and Measurement Noise Estimates^a

Elevation, deg	σ_i^m , mm	η_{WVR} , mm	η_{GPS} , mm				
			NOAA	Choke Rings	Filter	Multipath Map	Combined
10-15	0.66	2.28	1.45	1.47	1.07	1.40	0.97
15-20	0.51	1.17	1.17	1.28	0.88	1.22	0.81
20-25	0.44	0.70	1.08	1.06	0.85	0.92	0.72
25-30	0.43	0.56	0.76	0.76	0.62	0.73	0.57
30-35	0.33	0.47	0.71	0.53	0.46	0.53	0.45
35-40	0.29	0.45	0.72	0.57	0.53	0.50	0.45
40-45	0.24	0.45	0.64	0.49	0.46	0.45	0.41
45-50	0.22	0.44	0.58	0.42	0.39	0.35	0.31
50-55	0.20	0.41	0.59	0.44	0.40	0.40	0.36
55-60	0.15	0.31	0.44	0.31	0.28	0.30	0.26
60-65	0.14	0.36	0.36	0.31	0.29	0.30	0.26
65-70	0.15	0.37	0.47	0.30	0.28	0.28	0.25
70-75	0.00	0.40	0.49	0.30	0.27	0.27	0.24
75-80	0.12	0.30	0.42	0.26	0.23	0.26	0.22
80-85	0.09	0.37	0.18	0.19	0.16	0.15	0.13
85-90	0.04	0.31	0.18	0.22	0.19	0.20	0.14

^aRMS variation of the nonisotropic component of SW (column 2) and RMS errors for the WVR (column 3) and GPS (columns 4-8) observations as a function of elevation angle are shown in units of millimeters. The values are computed for all measurements within a 5° elevation bin. The GPS error estimates for the NOAA FSL station in Platteville are in column 4. The results presented in the remaining columns are from a combination of the two GPS stations in Platteville and Table Mountain that were equipped with 85 cm choke ring antennas. The data from these two stations without additional noise suppression are in column 5. The same two stations but with a 2 min filter applied are in column 6. The two stations using a multipath map are in column 7. The two stations with both a filter and multipath map applied are in column 8.

ish coastline, significantly larger than anything observed during this experiment.

As part of the GPS data analysis, estimates of PW and S_i^m were computed at the six NOAA FSL stations that were included in the analysis. While there was not a pointing radiometer at any of these stations, an analysis of their GPS-derived S_i^m observations indicates larger nonisotropic SW. In particular, three of the stations had S_i^m observations as large as 5 mm at elevation angles of 45°. Estimates of PW at these locations were in general also larger than those estimated at either Platteville or

Table Mountain. On the basis of comparisons between GPS- and WVR-derived S_i^m observations at Platteville and Table Mountain and previous studies that indicate that nonisotropic water vapor variability increases with increasing total water vapor content [Treuhaft and Lanyi, 1987], we interpret these as actual S_i^m observations.

Comparisons of GPS- and WVR-retrieved S_i^m measurements for individual satellite tracks are displayed in Figures 2 and 3. The GPS values are plotted in 30 sec intervals, while the WVR values are plotted approximately every 8 min. Once again, the portion of SW attrib-

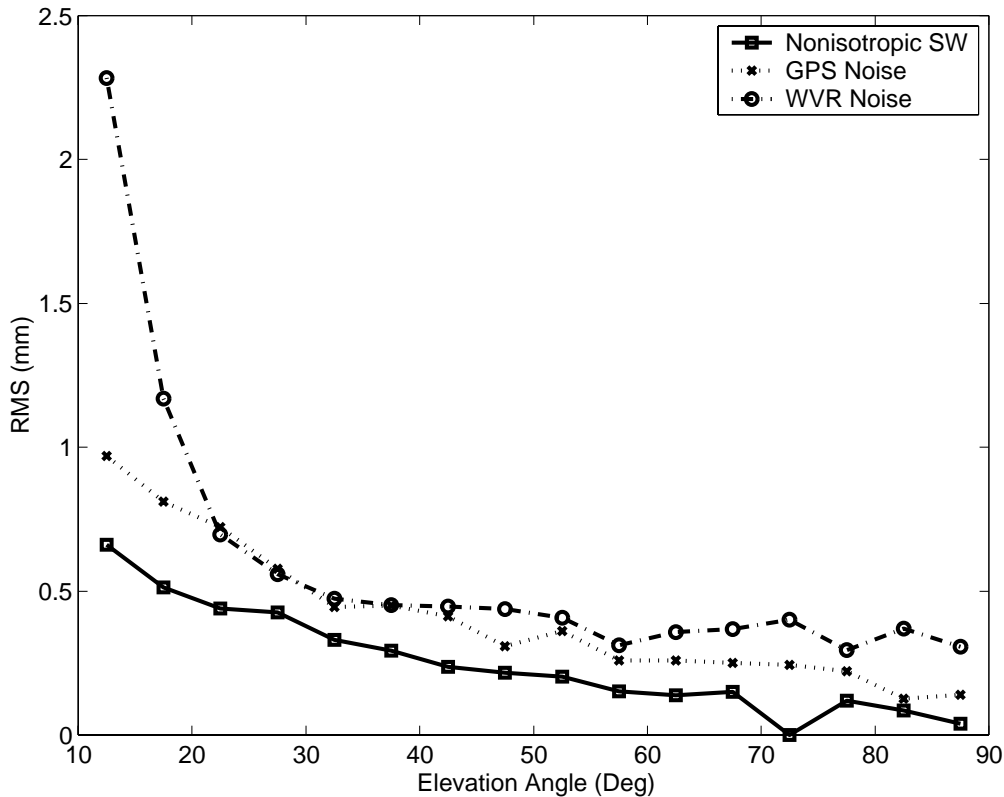


Figure 4. RMS of nonisotropic SW (solid line); GPS error using the choke ring antenna, multipath map, and 2 min filter (dotted line); and WVR error (dash-dotted line) as a function of elevation angle, in units of millimeters.

utable to the PW estimate has been removed. Figures 2 and 3 also show the coherence estimates between the GPS and WVR time series of S_i^m based on the Welch method of power spectrum estimation [Welch, 1967]. The examples shown in figures 2 and 3 have exceptionally high coherence estimates across all frequencies. The high coherence of the GPS and WVR time series indicates that while the noise level of the two techniques is relatively high, they have a common signal structure. This common signal is due to water vapor. In general, the times series of the other satellite tracks did not exhibit such high coherence across all frequencies, although they did show coherence of better than 0.5 across most frequencies (indicating that the two instruments observe the same nonisotropic slant water). This level of coherence between the two time series is reasonable considering that often, compared to the measurement noise of the two techniques, no significant water vapor heterogeneity is present.

5. Error Analysis

The value of SW measurements is their increased information on the spatial variability of water vapor in the atmosphere. A comparison of the nonisotropic component of the GPS and WVR SW observations allows for the determination of a reasonable error budget.

During this experiment the size of the nonisotropic component of SW, S_i^m , was generally the same order of magnitude as the size of the error in the two measurement techniques. In our simple error analysis we assume that the GPS errors, the WVR errors, and the nonisotropic component of SW were all zero mean, Gaussian, and independent from one another. The RMS of the GPS (σ_{iGPS}^m) and WVR (σ_{iWVR}^m) measurements of S_i^m can then be represented through (7) and (8)

$$\sigma_{iGPS}^m = [(\sigma_i^m)^2 + (\eta_{GPS})^2]^{1/2}, \quad (7)$$

$$\sigma_{iWVR}^m = [(\sigma_i^m)^2 + (\eta_{WVR})^2]^{1/2}, \quad (8)$$

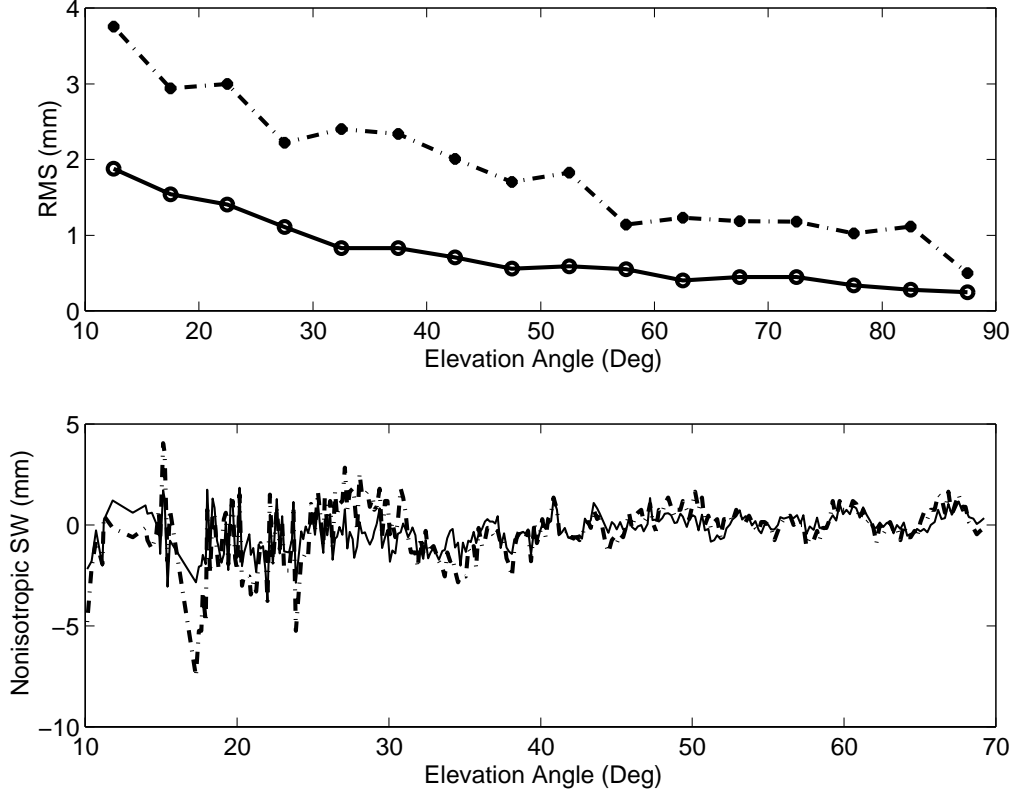


Figure 5. Double-difference (solid line) and precise-point-positioning (dashed line) RMS of nonisotropic SW as a function of elevation angle. Two example time series are plotted in the bottom panel. The residuals from double-difference analysis are plotted as the thin solid line, and the residuals from the point-positioning analysis are plotted as the thicker dash-dotted line.

where σ_i^m is the RMS variation of the actual amount of S_i^m common to both instruments and η_{GPS} and η_{WVR} are the respective GPS and WVR RMS measurement noise.

To statistically quantify the magnitude of S_i^m observed by the two instruments, the GPS and WVR observations were combined. First, the time series of the two measurements were added together. Note that we can manipulate the time series in this way because we are comparing instantaneous GPS and WVR observations of S_i^m at common epochs. The RMS of this time series contained twice the RMS amount of S_i^m in addition to the GPS and WVR RMS measurement noise

$$\sigma_{\text{GPS+WVR}} = [(2\sigma_i^m)^2 + (\eta_{\text{GPS}})^2 + (\eta_{\text{WVR}})^2]^{1/2}. \quad (9)$$

Second, the GPS and WVR time series were subtracted. The RMS of this time series contained only the noise in the two measurements

$$\sigma_{\text{GPS-WVR}} = [(\eta_{\text{GPS}})^2 + (\eta_{\text{WVR}})^2]^{1/2}. \quad (10)$$

The RMS size of actual nonisotropic SW common to both instruments could then be computed by squaring (9) and (10) and solving for σ_i^m

$$\sigma_i^m = \frac{1}{2} [(\sigma_{\text{GPS+WVR}})^2 - (\sigma_{\text{GPS-WVR}})^2]^{1/2}. \quad (11)$$

Once σ_i^m was determined, the RMS measurement noise of the GPS and WVR observations could also be computed

$$\eta_{\text{GPS}} = [(\sigma_{i\text{GPS}}^m)^2 - (\sigma_i^m)^2]^{1/2}, \quad (12)$$

$$\eta_{\text{WVR}} = [(\sigma_{i\text{WVR}}^m)^2 - (\sigma_i^m)^2]^{1/2}. \quad (13)$$

In our error analysis we grouped the observations by elevation angle and by individual satellite track. The values of σ_i^m , η_{WVR} , and η_{GPS} are plotted as a function of ele-

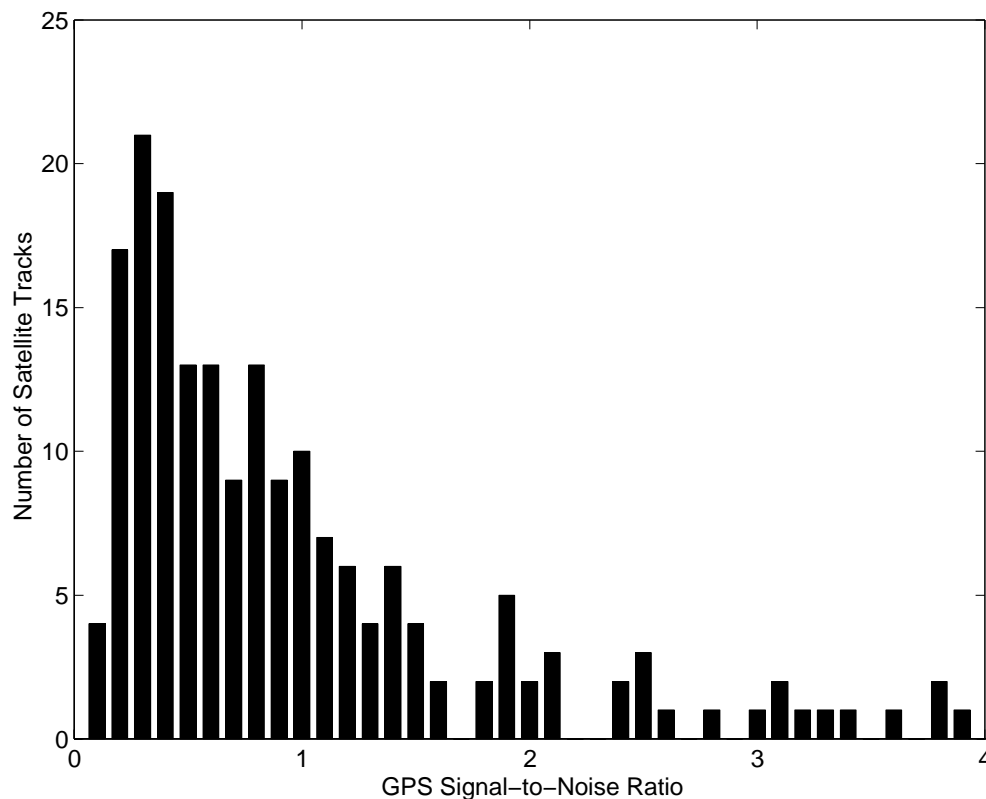


Figure 6. Histogram plotting the signal-to-noise ratio of the GPS-measured nonisotropic SW for all satellite tracks considered.

vation angle in Figure 4. These values are also shown in Table 1. Table 1 contains multiple columns for the GPS RMS measurement errors. Each column corresponds to a different technique that was used to reduce noise levels. Besides applying a filter for certain specified analysis techniques, the GPS and WVR results were compared without any type of time integration or averaging. The RMS of S_i^m common to both instruments is shown in column 2, and the WVR RMS measurement noise is shown in column 3. The Platteville location contained two stations: One was part of the NOAA FSL network, and one was the additional station with the 85 cm choke ring antenna. The RMS noise level of the data collected by the NOAA FSL station is given in column 4.

Columns 5-8 contain the combined analysis of data collected with the GPS instruments at both Platteville and Table Mountain using the 85 cm choke ring antennas. Neither station had significantly lower noise characteristics than the other. In column 5, the values are from data collected using the choke ring antennas without any addi-

tional type of noise suppression. There is a modest reduction in noise levels for observations above 30° elevation angle when compared to the data collected at the Platteville NOAA FSL station, which was equipped with a standard dielectric patch antenna with ground plane.

In one variation of the analysis a 2 min filter was applied to the GPS observations to improve the signal-to-noise characteristics of the GPS measurements. The length of the filter was chosen so that a sufficient number of observations could be used to reduce noise, while maintaining the instantaneous nonisotropic SW along the ray path between the satellite and the receiving antenna. As can be seen from column 6, the filter reduced the RMS measurement error for the lower elevation angles between 10° and 30° . These low-angle observations are typically more corrupted by ground-reflected multipath than higher-elevation-angle observations.

The effect of stacking of the 3 days of residuals in an attempt to reduce multipath is shown in column 7. Most of the improvement from the stacking of residuals was in

the elevation angles between 30° and 80° (column 7). This improvement was probably due to the removal of phase center variations between antennas, not to the elimination of multipath errors. The high-frequency multipath structure at lower elevation angles was probably not sufficiently well captured with a multipath map made from just 3 days of data. To further improve the results when compared to the filtering data, a larger number of days should be used when creating the map. *Alber et al.* [2000] identified significant levels of multipath reduction by using maps that were created by stacking data for more than a week.

Finally, when the filtering and multipath maps were used together (column 8), the RMS GPS noise levels showed improvement across all elevation angles, but most significantly at elevation angles below 30°. Like the results from column 6 where just the filter was applied to the observations, the improvement at these low elevation angles is due to the suppression of multipath.

6. Comparison of Double-Difference and Precise Point Position Processing

To compare results from PP and DD processing, data from a GPS station located in central Oklahoma were processed using both GPS analysis strategies. Both solutions were computed using a recently released version of the Bernese 4.2 software containing PP and DD capabilities. These data were collected in late December 1999. The 1996 data were not used for this analysis because satellite clocks were not available. The RMS variations of the nonisotropic SW are plotted in Figure 5 as a function of elevation angle. The time series for a single satellite using both processing strategies are also shown in Figure 5. There is high coherence between the PP and DD time series. However, the RMS variations of the PP line-of-sight residuals were at least twice as large as those of the DD strategy across all elevation angles. We therefore believe that the reduced RMS for the DD-derived nonisotropic SW is due to the elimination of receiver clock modeling. The residuals from both solutions contain multipath, antenna phase center variations, and atmospheric variability. These additional noise sources may significantly decrease the sensitivity of SW sensing using PP processing strategies.

7. Discussion

The variability in the nonisotropic component of the SW, S_i^m , and noise estimates for various elevation angles are provided in Figure 4 and Table 1. During the 3 days

of the experiment the RMS of the S_i^m observations increases from 0.1 mm near zenith to 0.6 mm at 10° elevation. This is smaller than the noise levels of both the WVR (0.3-2.3 mm RMS) and GPS (0.2-1.4 mm RMS) observations. We attribute the small nonisotropic RMS variations to the High Plains location of the experiment, to the lack of significant atmospheric variability at the time of the experiment, and to the elimination of WVR data during rainy periods when convective cells provided the largest S_i^m variability. We expect that an analysis of SW measurements in locations with higher and more variable PW values would also show an increase in the magnitude of the nonisotropic component of SW.

For each of the 183 satellite tracks considered, the GPS and WVR observations were combined to compute the RMS amount of nonisotropic SW, GPS observation noise, and WVR observation noise. The ratios of (11) and (12) were computed and can be considered to be a signal-to-noise ratio of the GPS observations over all elevation angles. A histogram of the ratios is shown in Figure 6. For this plot, approximately one third of the tracks had a signal-to-noise ratio of greater than 1, and more than half had a signal-to-noise ratio of greater than 0.8. This histogram illustrates that using the nonisotropic component of SW will oftentimes not introduce significant information in comparison to a single PW measurement. Complete SW measurements will only benefit weather prediction during conditions and locations where the nonisotropic water vapor structure is larger than the noise level of the observations. These conditions should occur during rapidly changing weather events associated with deep convection or frontal passage.

It is mentioned throughout this paper that GPS observations need to be accurately modeled to measure SW and S_i^m . Error budgets have been proposed in previous articles concerning the estimation of PW with GPS. In particular, this topic is discussed by *Bevis et al.* [1992]; and *Rocken et al.* [1993, 1997]. The error budgets outlined in these articles are valid for the sensing of SW observations and are not extensively discussed here. The errors discussed here will be the ones that most severely limit the measurement of S_i^m . These errors are caused by carrier phase noise, ground-reflected multipath, antenna phase center variations, and hydrostatic gradients in the atmosphere.

As can be seen from Table 1, the RMS error in the GPS S_i^m observations ranges from approximately 0.2 mm near zenith and increases to between 1.0 and 1.5 mm at elevation angles between 10° and 15°. High-accuracy dual-frequency GPS receivers, like the ones used in this

experiment, typically have RMS carrier phase noise levels in the ionospheric free linear combination of 1-1.5 mm. This corresponds to 0.15-0.23 mm of error in SW. Therefore an RMS error of 0.2 mm for S_i^m measurements near zenith implies that receiver noise is the principle error source at high elevation angles. Contributions from other error sources, such as mismodeling of the geometric component of the range measurement, or from errors introduced in the transformation of double-difference residuals into line-of-sight slant residuals [Alber *et al.*, 2000] are negligible at high angles. At low elevation angles the RMS error in S_i^m is as high as 1.4 mm. This corresponds to a delay measurement error of 9.1 mm. Low-elevation-angle observations are corrupted by multipath and antenna phase center errors. We attribute most of the additional increase in RMS noise of the GPS observations to these two error sources. Low-elevation-angle noise reduction requires improved multipath suppression in the GPS receivers and in postprocessing through site-specific phase correction maps like the ones outlined in section 3.2. We believe that these maps can be improved by using more days of observations (10 or more) in the computation of a map and by regularly updating the map to account for local variations in the multipath characteristics at a station.

One additional error that may affect low-elevation GPS slant water observations is the existence of horizontal gradients in the hydrostatic delay of the GPS signal. This topic has been previously considered by Chen and Herring [1997]. An investigation into such gradients during the data set presented in this paper revealed that there was a small hydrostatic gradient, particularly in the north-south direction, that may have contributed as much as 0.6 mm of RMS error for elevation angles near 10° . This is a significant error source and implies that the utilization of a mesoscale weather model may be needed to separate hydrostatic gradients from the actual SW.

In addition to errors in the GPS and WVR observations of S_i^m some of the discrepancy in the two measurement techniques can be attributed to the fact that the two instruments did not measure the exact same volume of atmosphere. The radiometer has a beam width of 5° , a much larger cross section than the GPS instrument whose beam width is approximated by the first Fresnel zone. At 3 km this corresponds to a 260 m beam width for the radiometer and a 54 m beam width for GPS. Any variability in the volume of atmosphere measured by the WVR would cause an error in the comparisons with GPS. Analysis of the GPS observations often showed significant changes in S_i^m over a time period of less than 8 min.

This indicates that the atmosphere contained spatial variations of water vapor that were smaller than the WVR could resolve. The difference in the volume of atmosphere sampled by the two instruments accounts for part of the RMS noise values presented in Table 1 and Figure 4.

The error budgets shown in Table 1 are derived from a rather limited data set taken from just 3 days of data at two High Plains locations. It is not possible to definitively obtain reliable uncertainties on these error estimates without collecting data from other locations and other time periods. However, the daily variability of the error estimates shown in Table 1 was approximately 15%. Therefore it should be reasonable to apply these empirically derived error estimates to data collected in other locations because the GPS errors will not scale with the total amount of water vapor observed by the instrument. The most important consideration when using these values at other locations will be the noise characteristics and multipath of the station. Data obtained from most of the permanently operating GPS stations will have characteristics similar to the ones reported by the NOAA FSL station (column 4). Any type of filtering of the data, or use of site-specific multipath maps, will further reduce the station-dependent errors, and the other columns may be used.

This analysis compares the precision in the measurement of the nonisotropic component of SW from two different instruments. If this analysis considered the absolute accuracy of the total SW measurement, it would be dominated by differences in the GPS- and WVR- measured isotropic components of SW. This is represented through the estimate of PW. Typical comparisons of GPS- and WVR-derived PW measurements show absolute RMS agreement of the two techniques to be 2 mm or better.

Because GPS senses water vapor on the basis of an excess delay, the error budget is based on the accuracy of a distance measurement. Errors will not scale with the total water vapor content in the atmosphere. Increased errors in S_i^m may arise in the conversion of double-difference residuals into line-of-sight slant water vapor delays. As discussed by Alber *et al.* [2000], errors in the line-of-sight slant water vapor delays may increase with increased spatial and temporal variability and can be minimized using a large network of receivers (more than 10) and with a network of GPS systems that is on the order of synoptic-scale weather features (a few hundreds of kilometers).

We expect that high-quality GPS measurements of SW can be obtained during nearly all weather conditions since the slant delays induced by hydrometeors and other particulates are generally negligible compared to delays induced by water vapor [Solheim *et al.*, 1999]. However, further validation of the method is needed during severe weather and for low elevation angles (below 10°). Further validation could be conducted via aircraft measurements during stormy conditions and via solar spectrometry [Sierk *et al.*, 1998] during clear conditions at low elevation angles.

8. Conclusions

We report a validation of GPS-derived slant water (SW) measurements by comparing the nonisotropic component of the SW measurement (S_i^m) to similar ones made using a water vapor radiometer. The comparison was made with 3 days of observations collected in Colorado during the late spring. The size of the observed nonisotropic component of SW was as large as 5 mm at an elevation angle near 10°. When these observations are scaled to their equivalent PW value, they correspond to less than 5% of the PW estimate. This indicates that the atmosphere was mostly isotropic during the experiment. The double-difference processing technique that was used in this analysis appears to offer increased sensitivity of S_i^m observations when compared to point-positioning analysis. This increased sensitivity is most likely due to the elimination of clock errors. The RMS noise level of the nonisotropic component of the GPS measurements was determined to be 0.2 mm of SW near zenith, equivalent to a 1.4 mm RMS noise level of the carrier phase (or slant water vapor delay) observations. At low elevation angles, where the contribution of errors from ground-reflected multipath and antenna phase center errors increases, the RMS GPS noise level rises to 1.4 mm, equivalent to 9.1 mm of RMS slant delay noise. If environmental noise is further suppressed, more precise measurements of S_i^m are possible. The technique of sensing SW has potential for real-time sensing of atmospheric water vapor for use in weather modeling and forecasting. In order to realize this potential, further validation of the method, including determination of its accuracy during severe weather and at low elevation angles, is needed.

Acknowledgments. Thanks are due to two anonymous reviewers, whose comments significantly improved this manuscript. The work presented here was supported by the Department of Energy Atmospheric Radiation Measurement (ARM) Program grant 354106 - AQ5, the National Center for Atmo-

spheric Research's (NCAR) Advanced Study Program (ASP), and the Office of Naval Research (ONR) grant N00014-97-1-0256.

9. References

- Alber, C., R. H. Ware, C. Rocken, and F. S. Solheim, GPS surveying with 1 mm precision using corrections for atmospheric slant path delay, *Geophys. Res. Lett.*, *24*, 1859-1862, 1997.
- Alber, C., R. H. Ware, C. Rocken, and J. J. Braun, Inverting GPS double differences to obtain single path phase delays, *Geophys. Res. Lett.*, *27*, 2661-2664, 2000.
- Beutler, G., I. Bauersima, W. Gurtner, M. Rothacher, T. Schildknecht, and A. Geiger, Atmospheric refraction and other important biases in GPS carrier phase observations, in *Atmospheric Effects on Geodetic Space Measurements*, Vol. 12, pp. 15-43, Sch. of Surv., Univ. of N. S. W., Kensington, N. S. W., Australia, 1988.
- Beutler, G., E. Brockman, S. Fankauer, W. Gurtner, J. Johnson, L. Mervart, M. Rothacher, S. Schaer, T. Springer, and R. Webber, Bernese GPS software version 4.0, Astron. Inst., Univ. of Bern, Bern, Switzerland, 1996.
- Bevis, M., S. Businger, T. A. Herring, C. Rocken, R. A. Anthes, and R. H. Ware, GPS meteorology: Remote sensing of atmospheric water vapor using the Global Positioning System, *J. Geophys. Res.*, *97*, 15,787-15,801, 1992.
- Bevis, M., S. Businger, S. Chiswell, T. A. Herring, R. A. Anthes, C. Rocken, and R. H. Ware, GPS meteorology: Mapping zenith wet delays onto precipitable water, *J. Appl. Meteorol.*, *33*, 379-386, 1994.
- Chen, G., and T. A. Herring, Effects of atmospheric azimuthal asymmetry on the analysis of space geodetic data, *J. Geophys. Res.*, *102*, 20,489-20,502, 1997.
- Dabberdt, F., and T. W. Schlatter, Research opportunities from emerging atmospheric observing and modeling capabilities, *Bull. Am. Meteorol. Soc.*, *77*, 305-323, 1996.
- Davis, J. L., T. A. Herring, I. I. Shapiro, A. E. Rogers, and G. Elgered, Geodesy by radio interferometry: Effects of atmospheric modeling errors on estimates of baseline length, *Radio Sci.*, *20*, 1593-1607, 1985.
- Davis, J. L., G. Elgered, A. E. Niell, and C. E. Kuehn, Ground-based measurement of gradients in the "wet" radio refractivity of air, *Radio Sci.*, *28*, 1003-1018, 1993.
- Elgered, G., J. L. Davis, T. A. Herring, and I. I. Shapiro, Geodesy by radio interferometry: Water vapor radiometry for estimation of the wet delay, *J. Geophys. Res.*, *96*, 6541-6555, 1991.
- Elosegui, P., J. Davis, I. Gradinarsky, G. Elgered, J. Johansson, D. Tahmoush, and D. A. Rius, Sensing atmospheric structure using small-scale space geodetic networks, *Geophys. Res. Lett.*, *26*, 2,445-2,448, 1999.
- Emanuel, K., et al., Report of the First Prospectus Development Team of the U.S. Weather Research Program

- to NOAA and the NSF, *Bull. Am. Meteorol. Soc.*, 76, 1194-1208, 1996.
- Guo, Y. R., Y. H. Kuo, J. Dudhia, D. Parsons, and C. Rocken, Four-dimensional variational data assimilation of heterogeneous mesoscale observations for a strong convective case, *Mon. Weather Rev.*, 128, 619-643, 2000.
- Gutman, S. I., D. E. Wolfe, and A. M. Simon, Development of an operational water vapor remote sensing system using GPS: A progress report, *FSL Forum*, Dec., 21-32, NOAA, Boulder, CO., 1995.
- Hanssen, R., T. Weckworth, H. Zebker, and R. Klees, High-resolution water vapor mapping from interferometric radar measurements, *Science*, 283, 1297-1299, 1999.
- Hogg, D., J. Guiraud, M. Snider, M. Decker, and E. Westwater, Measurement of excess radio transmission length on earth-space paths, *Astron. and Astrophys.*, 95, 304-307, 1981.
- Howe, B., K. Runciman, and J. Secan, Tomography of the ionosphere: Four-dimensional simulations, *Radio Sci.*, 33, 109-128, 1998.
- Jarlemark, P. O. J., T. R. Emardson, and J. M. Johansson, Wet delay variability calculated from radiometric measurements and its role in space geodetic parameter estimation, *Radio Sci.*, 33, 719-730, 1998.
- Kouba, J., 1997 Analysis Coordinator report, in *International GPS Service for Geodynamics, 1997 IGS Annual Report, JPL 400-786 10/98*, Jet Propul. Lab., Pasadena, Calif. 1998.
- Kuo, Y.-H. X. Zou, and Y.-R. Guo, Variational assimilation of precipitable water using a nonhydrostatic mesoscale adjoint model, *Mon. Weather Rev.*, 124, 122-147, 1996.
- MacDonald, A., and Y. Xie, On the use of slant observations from GPS to diagnose three dimensional water vapor using 3DVAR, paper presented at 4th Integrated Observing Systems Symposium, Am. Meteorol. Soc., Long Beach, Calif., Jan., 2000.
- Niell, A. E., Global mapping functions for the atmospheric delay at radio wavelengths, *J. Geophys. Res.*, 101, 3227-3246, 1996.
- Rocken, C., J. M. Johnson, R. E. Neilan, M. Cerezo, J. R. Jordan, M. J. Falls, L. D. Nelson, R. H. Ware, and M. Hayes, The measurement of atmospheric water vapor: Radiometer comparison and spatial variations, *IEEE Trans. Geosci. Remote Sens.*, 29, 3-8, 1991.
- Rocken, C., R. Ware, T. Van Hove, F. S. Solheim, C. Alber, and J. M. Johnson, Sensing atmospheric water vapor with the Global Positioning System, *Geophys. Res. Lett.*, 20, 2631-2634, 1993.
- Rocken, C., T. Van Hove, J. M. Johnson, F. S. Solheim, and R. H. Ware, GPS/STORM: GPS sensing of atmospheric water vapor for meteorology, *J. Atmos. Oceanic Technol.*, 12, 468-478, 1995.
- Rocken, C., T. Van Hove, and R. H. Ware, Near real-time GPS sensing of atmospheric water vapor, *Geophys. Res. Lett.*, 24, 3221-3224, 1997.
- Ruffini, G., L. Kruse, A. Rius, B. Burki, L. Cucurull, and A. Flores, Estimation of tropospheric zenith delay and gradients over the Madrid area using GPS and WVR data, *Geophys. Res. Lett.*, 26, 447-450, 1999.
- Sierk, B., B. Burki, L. P. Kruse, S. Florek, H. Becker-Ross, H. G. Kahle, and R. Neubert, A new instrumental approach for water vapor determination based on solar spectrometer, *Phys. Chem. Earth*, 32, 113-117, 1998.
- Solheim, F. S., R. Vivekanandan, R. H. Ware, and C. Rocken, Propagation delays induced in GPS signals by dry air, water vapor, hydrometeors and other atmospheric particulates, *J. Geophys. Res.*, 104, 9663-9670, 1999.
- Stokes, G. M., and S. E. Schwartz, The Atmospheric Radiation Measurement (ARM) Program: Programmatic background and design of the cloud and radiation test bed, *Bull. Am. Meteorol. Soc.*, 75, 1201-1221, 1994.
- Treuhaft, R. N., and G. L. Lanyi, The effect of the dynamic wet troposphere on radio interferometric measurements, *Radio Sci.*, 22, 251-265, 1987.
- Ware, R. H., C. Rocken, F. Solheim, T. Van Hove, C. Alber, and J. Johnson, Pointed water vapor radiometer corrections for accurate Global Positioning System surveying, *Geophys. Res. Lett.*, 20, 2635-2638, 1993.
- Ware, R. H., C. Alber, C. Rocken, and F. Solheim, Sensing integrated water vapor along GPS ray paths, *Geophys. Res. Lett.*, 24, 417-420, 1997.
- Welch, P. D., The use of fast fourier transfer for the estimation of power spectra: A method based on time averaging of short, modified periodograms, *IEEE Trans. Audio Electroacoust.*, AU-15, 70-73, 1967.
- Zhang, G., J. Vivekanandan, and M. Politovich, Scattering effects on microwave passive remote sensing of cloud parameters, paper presented at 8th Conference on Aviation, Range and Aerospace Meteorology, Am. Meteorol. Soc., Dallas, Tex., Jan. 1999.
- Zumberge, J. F., M. B. Heflin, D. C. Jefferson, and M. M. Watkins, Precise point positioning for the efficient and robust analysis of GPS data from large networks, *J. Geophys. Res.*, 102, 5005-5017, 1997.

J. Braun, C. Rocken, and R. Ware, GPS Research Group, UCAR, P. O. Box 3000, Boulder, CO 80307. (braunj@ucar.edu; rocken@ucar.edu; ware@ucar.edu)

(Received March 24, 2000; revised September 18, 2000; accepted October 17, 2000.)

Copyright 2001 by the American Geophysical Union.

Paper number 2000RS002353.
0048-6604/01/2000RS002353\$11.00